RSC Advances

PAPER

View Article Online
View Journal | View Issue

Cite this: *RSC Adv.*, 2020, **10**, 23624

Characterization of the structure–function relationship of a novel salt-resistant antimicrobial peptide, RR12†

Ping-Sheng Wu,[a] Shu-Jung Lai,[bd] Kit-Man Fung[b] and Tien-Sheng Tseng *[c]

Received 14th May 2020
Accepted 15th June 2020

DOI: 10.1039/d0ra04299d

rsc.li/rsc-advances

Antimicrobial peptides (AMPs) are potential candidates in designing new anti-infective agents. However, many AMPs show poor bactericidal activities in physical salt and serum solutions. Here, we disclosed the structure–function relationships of a novel salt-resistant antimicrobial peptide, **RR12**, which could further explain its mode of action and show its applicability in developing new antibacterial agents.

Introductions

The rapid emergence of antibiotic-resistant bacteria is now a severe health problem all around the world.[1,2] Therefore, developing new bactericidal agents with less probability to induce evolved resistance is urgently needed. In nature, organisms genetically obtain abilities from progenitors to defend themselves against pathogens. Their immune resistant abilities are connected to the development of specific immune responses. Antimicrobial peptides (AMPs) are the natural element of the innate immune system observed in most living organisms.[3–5] AMPs target and disrupt the plasma membrane of bacteria leading to death, and have a minimal inhibitory concentration against bacteria in the μM range.[6–8] Thus, AMPs are feasible candidates in developing potent therapeutics against the infections of antibiotic-resistant bacteria.

Nowadays, thousands of AMPs are characterized and deposited in the Antimicrobial Peptide Database (AMSDb, http://aps.unmc.edu/AP/main.php). The database can be used to predict the structure, function, and antibacterial activities on the basis of peptide sequence.[9–11] AMPs mostly present as amphipathic peptides (12–30 amino acids) containing positive charges from +2 to +9 with some hydrophobic residues.[7,12,13] Structurally, AMPs are observed in four types: α-helical, β-sheet, loop, and extended peptides.[13,14] In particular, the α-helical conformation is the most effective structural arrangement observed at the bacterial surface in innate defense.[15] Functionally, AMPs possess two important features: (1) the capability of assuming an amphipathic helical conformation—most AMPs are linearly unstructured and fold into an amphipathic helix when targeting to bacterial membrane—and (2) a net cationicity—cationic AMPs bind to the negative-charged bacterial surface.[13,16–20] With these properties, AMPs can disrupt the transmembrane potential, interfere the balance of ion gradients, and cause the leakage of cell contents, finally leading to microbial death.

To be molded into potent bactericidal agents, AMPs should have less hemolytic activities and effective bactericidal abilities. However, high amphipathicity and hydrophobicity of AMPs are reported to be correlated with high hemolytic activity.[21] Additionally, natural AMPs show low bioavailability and are easily degraded by proteases.[22,23] Therefore, shorter peptides were modified to enhance the antimicrobial activity but decrease hemolytic activity and cytotoxicity.[24–27] While many natural AMPs still exhibit poor bactericidal abilities in physical salt concentrations.[28,29] This significantly hindered the pharmaceutical development of AMPs as new therapeutic agents. Thus, investigation and development of AMPs with strong salt tolerance and antibacterial activities are essential in combating antibiotics-resistant bacteria.

Recently, Harini Mohanram *et al.* reported a peptide, **RR12** (RRLIRLILRLLR), exerting bactericidal activity and is not affected by high concentration of sodium chloride (150–300 mM) or 10% human serum containing media.[30] Although **RR12** was observed to interfere membrane integrity of *E. coli* cells in the presence of salt, detailed characterizations of its structure–function relationships have not been thoroughly investigated. The development of biocidal AMPs is usually hindered by poorly understanding of information on their physicochemical characteristics, which are highly associated with their mode of actions.[31,32] Therefore, to disclose the bactericidal function of **RR12**, we investigated its structural properties, capability of interacting with membranes, and the solution structure on binding with membrane-mimetic micelles.

[a]*Division of Infectious Diseases, Department of Pediatrics, Taipei Tzu Chi Hospital, Buddhist Tzu Chi Medical Foundation, New Taipei, Taiwan*

[b]*Institute of Biological Chemistry, Academia Sinica, Taipei 115, Taiwan*

[c]*Institute of Molecular Biology, National Chung Hsing University, Taichung, Taiwan*

[d]*Graduate Institute of Biomedical Sciences, China Medical University, Taichung, Taiwan*

† Electronic supplementary information (ESI) available. See DOI: 10.1039/d0ra04299d

Here, we employed biochemical and biophysical techniques to study the characteristics of **RR12** in interacting with sodium dodecyl sulfate (SDS) micelles. We performed Far-UV CD, dye-leakage fluorescence assay, 2D and spin-labeling NMR to investigate the secondary structure content, membrane-permeabilizing activity, solution structure, and orientation in SDS micelles, respectively. The observed structural and functional insights could explain the mechanism of action of **RR12** against microbes and provide valuable information for development of new anti-infective agents with salt-resistant abilities.

Materials and methods

Materials

RR12 peptide (RRLIRLILRLLR-amide) was synthesized by Yao-Hong Biotechnology Inc (http://www.yh-bio.com.tw/en/index.asp). 1-palmitoyl-2-oleoyl-*sn-glycero*-3-phosphocholine (POPC) and 1-palmitoyl-2-oleoyl-*sn-glycero*-3-phosphoglycerol (POPG) were from Avanti Polar Lipids (Alabaster, AL, USA). Calcein, $MnCl_2$ and 5-, and 12-doxyl stearic acids were from Sigma-Aldrich. SDS-d_{25}, methanol-d_4 and D_2O were from Cambridge Isotope Laboratories. Sodium dodecyl sulfate was from Merk (Darmstadt, Germany).

Methods

Circular dichroism (CD) spectroscopy. Far-UV CD experiments were carried out by using a Chirascan-Plus CD Spectrometer (Applied Photophysics Ltd, Leatherhead, UK). **RR12** was dissolved in 10 mM sodium phosphate buffer (pH 5.0) to yield a 1.5 mM stock. CD samples were prepared by diluting the peptide stock into TFE, DPC, and SDS separately to reach the concentrations and molar ratios of interest (**RR12** (60 μM) in 10, 20, and 50% TFE; **RR12** : DPC = 1 : 100 (molar ratio), and **RR12** : SDS = 1 : 100 (molar ratio)). Far-UV CD experiments were conducted by using a 1 mm path length quartz cuvette at 25 °C with the observed wavelength range between 190 and 260 nm. All spectra were averaged over three scans and converted to mean residue ellipticity [θ]. The helical contents of all spectra were estimated by using BESTSEL (http://bestsel.elte.hu/).

Preparation of large unilamellar vesicles (LUVs). The LUVs were prepared according to previous description.[33] The phospholipids (POPC and POPG) were liquefied with chloroform and dried by nitrogen air. The dried lipid film was liquefied in phosphate buffered saline (PBS) buffer (137 mM NaCl, 2.7 mM KCl, 10 mM Na_2HPO_4, 1.8 mM KH_2PO_4, pH 7.4) and followed by 10 rounds of freezing and thawing. The generation of LUVs is as follows: lipid suspensions were extruded by using a mini-extrusion device (Avanti Polar Lipids, Alabaster, AL, USA) through two stacked 0.4 μm pore-size polycarbonate filters 10 times, then extruded with two stacked 0.1 μm pore-size filters for another 10 times. Likewise, the calcein-entrapped LUVs were generated in the calcein-containing buffer (70 mM calcein, 10 mM Tris, pH 7.4) with the same process mentioned above. Subsequently, the un-entrapped calcein was removed by centrifugation (10 000 rpm for 10 min) three times by using isosmotic buffer (10 mM Tris and 100 mM NaCl, pH 7.4). The size of the generated LUVs was confirmed by dynamic light scattering on a Zetasizer Nano ZS (Malvern Instruments, Malvern, UK).

Calcein leakage assay. The peptide-induced calcein leakage assays were conducted by using a JASCO FP-8500 spectrofluorometer (JASCO, Tokyo) with excitation = 496 nm and emission = 515 nm. Measurements were involved ~30 μM lipids of calcein-entrapped LUVs in 20 mM Tris and 100 mM NaCl, pH 7.4 at 25 °C. The 100% leakage was induced by the addition of 0.1% (v/v) Triton X-100. The degree of leakage induced by distinct concentrations of peptides was determined after 10 minutes incubations of peptide and calcein-entrapped LUVs by the following equation: % leakage = $[(F - F_0)/(F_r - F_0)] \times 100$. ($F_0$ and F_r are the fluorescence intensities observed without peptide and with Triton X-100 treatment, respectively.)

NMR spectroscopy. The samples for NMR experiments were prepared by mixing **RR12** (final concentration 1.5 mM) with SDS (final concentration 150 mM) to reach a molar ratio of 1 : 100, containing 10 mM sodium phosphate and 10% D_2O at pH 5.0. All NMR experiments involved Bruker Avance 600 and 800 MHz spectrometry at 310 K. 2D-NOESY spectra were acquired at two distinct mixing times of 150 and 300 ms. TOCSY spectra were recorded with mixing time 60 ms at 2048 points in t_2 and 320 points in t_1. A natural-abundance (^{1}H, ^{15}N) HSQC spectrum[34] was obtained at 2048 points in t_2 and 400 points in t_1. The spectra were processed by using TopSpin 3.1 (Brucker Spectrospin) and NMRPipe.[35] Sparky (T. D. Goddard and D. G. Kneller, University of California, San Francisco) was employed for spectra analysis.

Structure calculation. 2D-NOESY spectra (mixing time: 150 ms) for **RR12** in SDS micelles (molar ratio = 1 : 100) were acquired at pH 5.0, 310 K and then subjected to manually assignments to obtain distance constraints. Based on the peak intensity, the NOE cross-peaks were clustered into strong, medium, and weak, corresponding to a distance range of 1.8–2.8, 1.8–3.4, and 1.8–5.0 Å, respectively. The backbone dihedral angle constraints were deduced from the ^{1}H and ^{15}N chemical shifts of natural-abundance HSQC spectra by using TALOS.[36,37] The solution structures were calculated by using CNS 1.2 for restrained molecular dynamic simulations.[38,39] The 20 lowest energy structures were examined by using PROCHECK-NMR[40] and MOLMOL.[41] PyMol (http://www.pymol.org) was employed for molecular visualization.

Paramagnetic relaxation enhancement (PRE) experiments. PRE experiments were performed in the presence of aliquots of Mn^{2+}, 5-doxyl-stearic acid (5-DSA) and 12-doxyl-stearic acid (12-DSA) in the NMR sample. $MnCl_2 \cdot 4H_2O$ was dissolved in 10 mM sodium phosphate pH 5.0 to prepare Mn^{2+} ion solution (0.1 M). To estimate the PRE effects, the Mn^{2+} ions were added to final concentration of 0.5 mM in the **RR12**–SDS micelle solution (molar ratio = 1 : 100) and equilibrated for 15 min before ^{1}H–^{1}H TOCSY spectra recording. For the PRE experiments of DSA, the DSA powders were dissolved in deuterated methanol (D_4-MeOH). The DAS solution was then mixed with SDS (in 10 mM sodium phosphate, pH 5.0) at a molar ratio of 1 : 60. Subsequently, **RR12** was added to the prepared DSA–SDS mixed

micelle solution. The final concentrations of DSA, SDS and **RR12** were 2.5, 150, and 1.5 mM, respectively. These NMR samples were equilibrated for 15 min before ^{1}H–^{1}H TOCSY experiments. The ^{1}H–^{1}H TOCSY spectra were acquired with the same parameters (310 K with 2048 data points in t_2 and 320 points in t_1) except for the probe tuning and field shimming. The cross-peak intensities of **RR12** were measured and calculated based on the protocol.[42]

Results

The secondary structure of RR12 in membrane mimic environment

We employed Far-UV CD spectroscopy to investigate the secondary structure of **RR12**. The CD spectra of **RR12** showed a random coil conformation in buffer (10 mM sodium phosphate, pH 5.0). While, the spectra for **RR12** in 50% TFE displayed strong signals at 208 and 222 nm (α-helical content = 51.6%) (Fig. 1). When interacting with DPC micelles (molar ratio of peptide : DPC = 1 : 100), **RR12** showed a bit increased helicity (α-helical content = 57.3%), compared to that in 40% TFE. When interacting with SDS micelles (molar ratio of peptide : SDS = 1 : 100), **RR12** exhibited comparable α-helical content (62%) to that in DPC micelles.

Solution structure of RR12 in complex with SDS micelle

We conducted NMR experiments to determine the solution structure of **RR12**. **RR12** showed well dispersed and high resolved spectra (2D-NOESY and TOCSY) in SDS micelles at pH 5.0 and 310 K (Fig. S1†). Therefore, the solution structure of **RR12** was determined in SDS micelles. The sequential assignments were completed by using 2D-TOCSY and NOESY spectra. The 200 NOE-derived distance constraints contained 96 intra-residue, 49 sequential, and 55 medium-range distance restraints. Besides, 18 backbone dihedral angle restrains derived from ^{1}H, ^{15}N- HSQC spectrum (Fig. 2A) were employed for structure calculation of the SDS micelle-bound **RR12** (Table 1). The superimposed ensemble of the 20 lowest-energy structures is shown in Fig. 2B. The root mean square deviations (RMSD) of top10 lowest-energy coordinates are 0.7 ± 0.17 Å for all heavy atoms and 0.3 ± 0.13 Å for backbone heavy atoms (Table 1). Moreover, a Ramachandran plot of PROCHECK analysis demonstrated that 70% and 30% of **RR12** residues are located at the most favored and additionally allowed regions, respectively. The structure of **RR12** is composed of a two-turn α-helix (L3-L11) with the loop conformations at N- and C-termini (Fig. 2C). Notably, the structure along with the electrostatic surface (Fig. 2D) of **RR12** revealed that positive-charged side chains of arginine residues (R1, R2, R5, R9, and R12) are on one side of the helix and the hydrophobic side chains are on the other side, revealing the apparent amphipathicity of **RR12**.

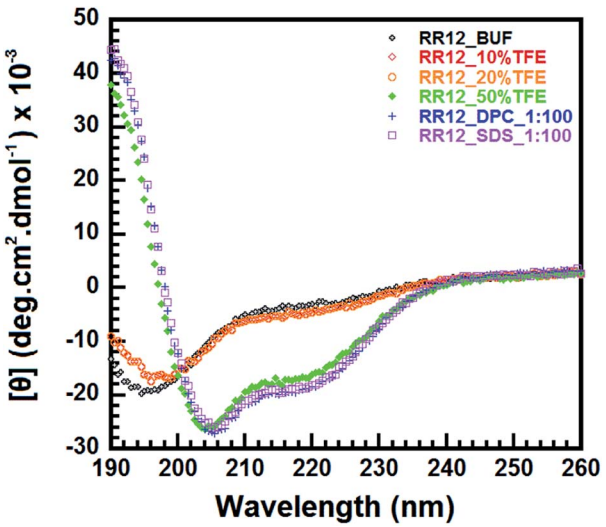

Fig. 1 Far-UV CD spectra for **RR12** in TFE, DPC and SDS micelles.

Membrane-permeabilizing ability of RR12 against synthetic LUVs

The peptide-induced leakage of calcein entrapped in LUVs of different surface-charge densities was employed to evaluate the membrane-permeabilizing ability of **RR12**. The highly negative-charged POPG and neutral POPC LUVs were used to mimic the bacterial and eukaryotic cell membranes, respectively. The minimal concentration of **RR12** causing 100% leakage of calcein from the LUVs is termed as LC100. **RR12** induced The LC100 of **RR12** against POPG LUVs was 0.008 μM (Fig. 3). However, the LC100 of **RR12** against POPC LUVs was 0.2 μM. These indicated that **RR12** has stronger disrupting ability against negative-charged bacterial membranes but much weaker activity against neutral charged eukaryotic cell membranes.

Localization of RR12 in SDS micelles. The PRE experiments were further performed to probe the position and orientation of **RR12** in SDS micelles. The 5- and 12-DSAs (spin-labeled fatty acids), with the paramagnetic doxyl-group at the 5th and 12th carbon positions of the acyl chain were utilized. 5-DSA influences the NMR signals of NH–C$_\alpha$H near the surface of the micelle; 12-DSA perturbs the signals of NH-C$_\alpha$H inserted into the micelle. The signals of NH–C$_\alpha$H resonances in TOCSY (F2 dimension) were employed to calculate the relative decreased intensities, compared to those of the peptide without spin label effects in SDS micelles. The result showed that the mean remaining amplitudes of **RR12** in the presence of 5- and 12-DSAs were 55% and 50%, respectively (Fig. 4A). Obviously, Residues R2–I7 were much affected by 12-DSA than 5-DSA, hence this segment is probably inserted into the SDS micelles. Whereas the remaining amplitudes of the C-terminus (R9–R12) were mostly higher than the average, implying that C-terminus could be outside SDS micelles and exposed to the solvent. To confirm the position of C-terminal residues R9–R12, the PRE experiment was conducted in the presence of 0.5 mM Mn^{2+} ions. Mn^{2+} ion can interact with the sulfate group of SDS, broadening the NMR resonance and decreasing the intensities of the nearby nucleus. The result showed that the peak intensities of residues R9–R12 were significantly reduced with the addition of Mn^{2+} ions (Fig. 4A). This revealed that the C-

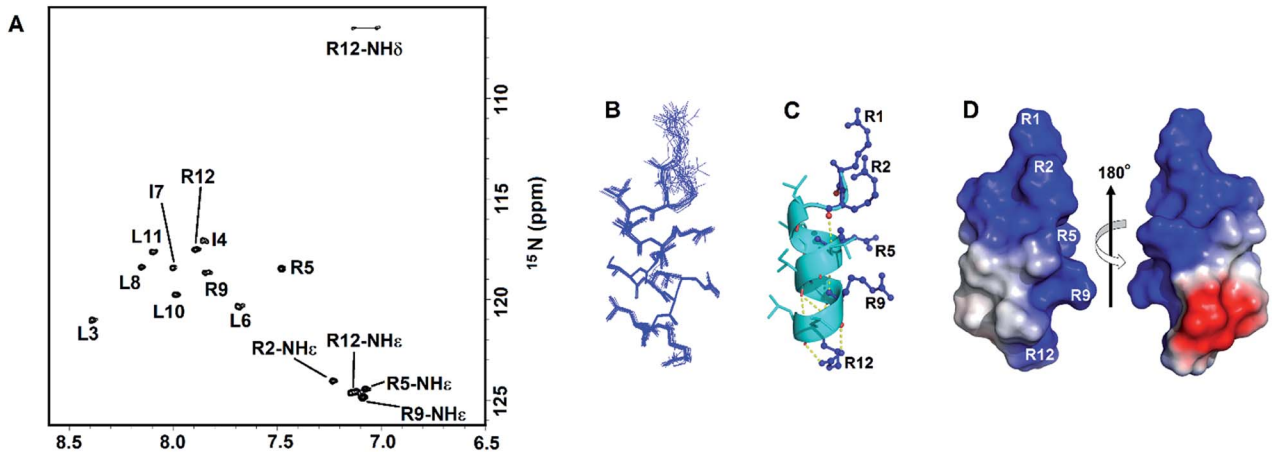

Fig. 2 NMR spectra and solution structure of **RR12** in SDS micelles (PDB ID: 6J9P). (A) The $^{1}H-^{15}N$ HSQC spectrum of **RR12** in SDS micelles. (B) Superposition of the 20 lowest energy structures of **RR12**. The backbones and heavy chains are shown in blue lines. (C) Ribbon representation of the averaged SDS-bound solution structure. Arginine residues in blue are shown as balls and sticks. (D) The electrostatic surface of SDS-bound **RR12**.The positive charge is in blue, negative charge in red, and neutral positions in white.

Table 1 NMR structure calculation parameters (PDB ID : 6J9P)[a]

NOE restraints	
Intra-residue NOEs	96
Sequential NOEs $[(i-j)=1]$	49
Medium-range NOEs $(\lvert i-j\rvert \leq 4)$	55
Total NOEs	200
Dihedral angle restraints	18
Ramachandran plot summary (%)	
Most favored	70
Additionally allowed	30
Generally allowed	0
Disallowed	0
Average RMSD from the mean structure	
Back atoms	0.3 ± 0.13
All heavy atoms	0.7 ± 0.17

[a] The default parameters and force constants of protein allhdg.param and anneal.inp in CNS1.2 are employed for the structure calculations. There are no NOE and dihedral angle violations observed during the structure calculations.

terminus is outside the SDS micelles. Accordingly, we built the possible model of **RR12**–SDS–micelles complex (Fig. 4B) on the basses of the determined solution structure of **RR12** and the PRE results.

Discussion

The broad-spectrum antibiotics have been the major components for antibacterial therapy. While the rapid emergence of antibiotic-resistant bacteria forced to reconsider new strategies in combating pathogenic microbes. The AMPs are promising candidates in developing new anti-infective agents.[43] Nevertheless, many AMPs exert limited bactericidal activities in physical salt and serum solutions.[44] Thus, AMPs with salt-resistant capabilities are urgently required for developments of future antibiotics. A short AMP, **RR12**, was demonstrated exhibited antibacterial activity in the presence of NaCl (150 and 300 mM) and human serum, but its characteristics in terms of structure and function are not clearly investigated. Here, we used biochemical and biophysical methods to investigate the structure–function relationship of **RR12** in SDS micelles to understand the possible mode of action.

We characterized the structural properties of **RR12** associated with its antimicrobial function through CD spectroscopy. **RR12** is a random coil in phosphate buffer solution but shows apparent α-helical structure in 50% TFE. Fluorinated alcohol can change the electrostatic interactions of the peptides and affect the carbonyl and amide groups, enhancing the hydrogen bond formation to stabilize helical formation.[45–47] **RR12** also adapted the α-helical conformations in both zwitter-ionic DPC and negative-charged SDS micelle systems (Fig. 1), indicating the bioactive conformational transition (from unstructured to α-helical conformation) of **RR12** is required for binding to phospholipid membranes. This observation is consistent with previous report that AMPs are disordered in aqueous conditions but become structured upon interacting with phospholipid membranes.[19,48,49] To understand the structural basis for the mechanism of action of **RR12** when interacting with bacterial membranes, we determined its solution structure by solution NMR. The synthetic peptide, **RR12**, was soluble and stable at acidic environment (pH 5.0) with high concentration (>2 mM). However it easily precipitated when dissolved or titrated to more basic environments (pH 7.0). The **RR12** peptide solution was observed clear without precipitates at 1–300 μM but gradually get aggregated when the concentration was over 500 μM at pH 6.5–7.0. Thus, we acquired 1D and 2D NMR spectra of **RR12** in zwitterionic DPC and negatively charged SDS micelles at pH 5.0 (Fig. 2A and S2–S4†). SDS micelles consists of a negatively charged outer surface and a hydrophobic inner core, thus mimicking the bacterial cell membranes.[50,51] The spectra (2D-

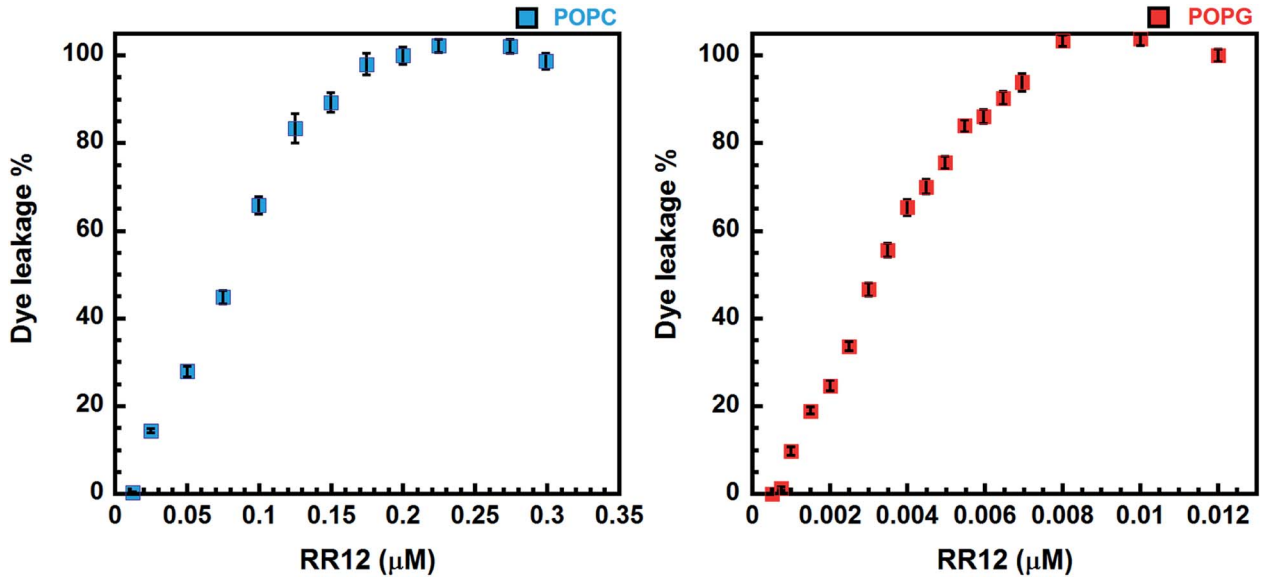

Fig. 3 Calcein leakage caused by **RR12** against the POPC and POPG LUVs.

TOCSY and NOESY) of **RR12** in SDS micelles are well-dispersed and highly resolved than those of in DPC micelles. To directly and successfully investigate the interactions between **RR12** and micelles, we simplified the solvent condition to a phosphate buffer at pH 5.0 (10 mM) without salt effect. The obtained solution structure represents an initial scaffold and conformation of **RR12** which is able to exert its salt-resistant ability. Thus, we finally determined the solution structure of **RR12** in complex with SDS micelles. Structurally, residues L3–L11 of **RR12** display an amphipathic α-helical conformation with hydrophobic and positive charged side chains positioned at opposite sides (Fig. 2).

Generally, short and small AMPs exert the bactericidal activities through binding and disrupting the integrity of microbial membrane.[7,52,53] Especially, the cationic residues of amphipathic helical AMPs are critical in interacting with the negatively charged and lipidic components of microbial membranes.[19,54] Therefore, we compared the structure of **RR12**

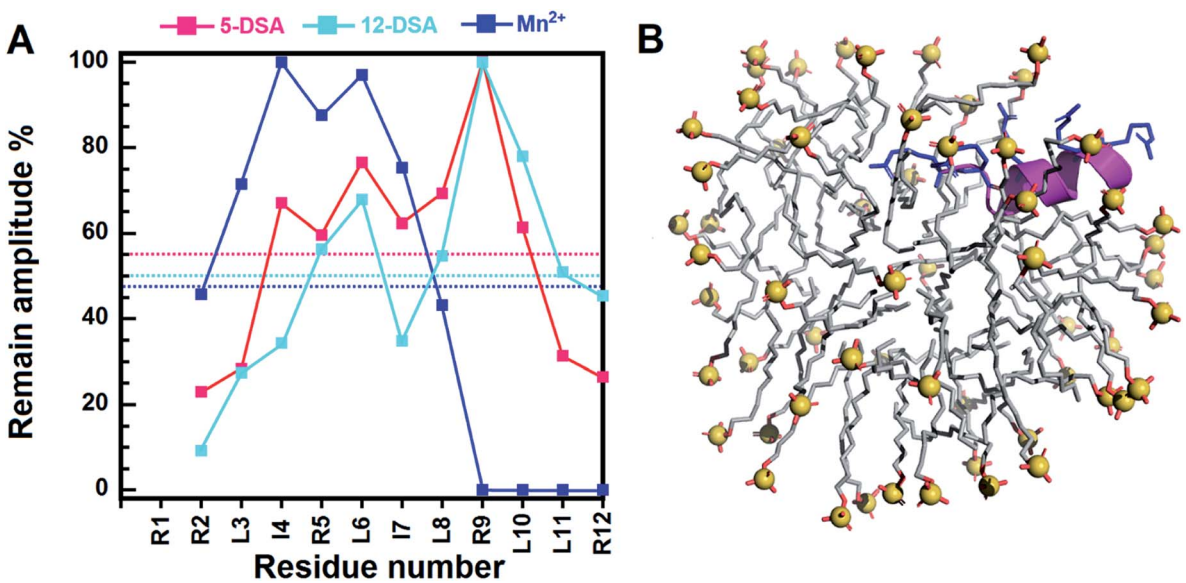

Fig. 4 The position of RR12 in SDS micelles. (A) The remaining amplitudes of NH–C_αH cross peaks derived from the TOCSY spectra of **RR12** due to 5- and 12-DSAs. The concentration of each DSA corresponds to a spin label per micelle. The magenta, cyan, and blue dotted lines indicate the mean remaining amplitudes of **RR12** in the presence of 5-, 12-, and (0.5 mM) Mn^{2+} ions, individually. (B) The model structure of **RR12** in complex with SDS micelle deduced from PRE results. The **RR12** peptide was shown as magenta ribbon with arginine residues and R1, R2, R5, R9 and R12 presented in blue sticks. The SDS lipids were displayed as light-grey sticks with the sulphur atoms shown as spheres (yellow) and oxygen atoms were colored in red.

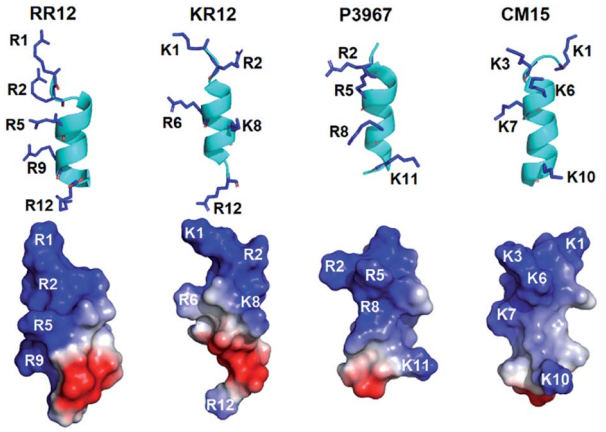

Fig. 5 Structural comparisons of RR12 with the known AMPs.

with those of known short AMPs (Fig. 5) to understand the possible mode of action of **RR12**. The AMPs, **KR12** (from human cathelicidin LL-37 (PDB ID : 2NA3)), **P3967** (from medicinal leech *Hirudo medicinalis* (PDB ID : 6RRL)), **CM15** (a hybrid peptide of Cecropin1-8 + Melittin3-9 (PDB ID : 2JMY)), and are 12, 12, and 15 in lengths. The structures of these AMPs are mostly amphipathic helices (Fig. S5†), however the distributions of their cationic residues are varied. **RR12**, **KR12**, **P3967**, and **CM15** show similar 2–3 turns α-helical conformations with the positively charged resides (arginine and lysine) extrude outwards. In **KR12**, K1, R6, and R12 are on the same side while the side chains of R2 and K8 slightly orient in distinct directions. Similar characters were observed in the structure of **P3967** (R2, R5, and R8 are nearly on the same side; K11 extrudes oppositely) and **CM15** (K1 and K10 orient in the same direction; K3 and K7 are on the same side; K6 positions in between). In contrast, the side chains of all the positive charged residues of **RR12** (R1, R2, R5, R9, and R12) orient in the same direction, exhibiting high amphipathicity. It has been reported that the designed, arginine-based peptides showed improved salt resistance bactericidal activity[55] and the cation–π interaction of arginine is highly associated with.[56] Accordingly, arginine residues aligned on the cationic side of **RR12** is of great potential to render its salt resistant ability-due to the possible ionic and hydrogen bonds interactions towards the bacterial outer membranes.

Functionally, **RR12** exerts stronger ability in disrupting negatively charged phospholipid vesicles (POPG) as shown in our dye leakage assay (Fig. 3). **RR12** can cause 100% calcein leakage at peptide concentration of 0.008 and 0.2 μM against POPG and POPC LUVs, respectively, revealing the selectivity of **RR12** against bacterial membranes instead of mammalian cells. Consequently, the α-helix (L3–L11) induced by the presence of SDS micelles is essential in membraned permeability as well as the bactericidal ability. Consistently, the strong membrane disrupting activity of **RR12** can also be seen from its broad bactericidal abilities against Gram-positive bacteria (*Bacillus subtilis*, *Staphylococcus aureus* (ATCC25923), and *Staphylococcus aureus* (ATCC25923)) and Gram-positive bacteria (*Salmonella enterica* (ATCC14028), *Pseudomonas aeruginosa* (ATCC27853), and *Klebsiella pneumoniae* (ATCC13883)).[30]

Most AMPs are prone to bind to the interfacial region of bacterial membranes with its polar face exposed to the solvent and the hydrophobic face embedded in the membranes.[15,57–59] Our NMR paramagnetic experiments were performed with 5-DSA, 12-DSA, and Mn^{2+} ions (Fig. 4 and S6–S8†). Mn^{2+} can cause broadening of resonances of residues which are near the surface of micelles or exposed to the solvents. For the 5-DSA, it broadens the signals of resonances of residues situated near the micellar boundary, whereas the spin label of 12-DSA will result in the reduction of peak intensity of resonances near to the center of the micelle.[60–62] In SDS micelles, the C-terminal residues of **RR12** were considerably affected by Mn^{2+} ions, with cross peaks of R9, L10, L11, and R12 completely disappearing in the 2D-TOCSY spectrum (Fig. S8†), indicating that the C-terminus lies at the surface or lies outside the micelles. Apart from the R9–R12, the remaining residues (R2–L8) were obviously affected by both 5-and 12-DSAs. This could be explained by the fact that micelles are mobile and continuously change, altering their positions and shapes in the solutions. The flexibility of micelles and the hydrophobic tails of 5- and 12-DSAs make it difficult to clearly distinguish the effects of the two probes.[63] This resulted in similar broadening effects for most of the resonances of residues buried inside the SDS micelles. Accordingly, the segment (R2–L8) of **RR12** is more buried, probably with the positively charged residues (R2, R5, and R9) facing the inner surface of micelle and the hydrophobic residues oriented into the micelle's interior. It has been reported that the α-helicity of AMPs is important for the dye-leakage abilities and antimicrobial activities.[64] Thus, the induced α-helical segment (R2–I7) of **RR12** upon interacting with SDS micelles is essential for membrane permeabilization and bacteriostatic activity.

Conclusions

In this study, we characterized the bioactive structure and function of the salt-resistant AMP, **RR12** by biophysical and biochemical examinations. **RR12** shows conformational transition (disordered coil to well-defined α-helix structure) when interacting with SDS micelles. We determined the detail solution structure of **RR12** in complex with SDS micelles. **RR12** orients itself into SDS micelles, with R2–I7 buried and C-terminus (R9–R12) exposed to the solvent. **RR12** shows well selectivity against negative-charged bacterial membranes, particularly, its α-helix segment (L3–L11) could significantly contribute in membrane permeabilization and bactericidal activity. Taken together, our study disclosed the structural and functional properties/relationships of **RR12** which could further explain its possible mode of action and shows the applicability in developing new antibacterial agents.

Conflicts of interest

There are no conflicts to declare.

Acknowledgements

We acknowledge the use of the Chirascan-Plus CD Spectrometer in the Biophysics Core Facility, Department of Academic Affairs and Instrument Service at Academia Sinica. We also acknowledge the acquisition of NMR spectra at the High-field Biomacromolecular NMR Core Facility, Academia Sinica. The study was supported by the Ministry of Science and Technology, Taiwan, ROC (MOST 108-2320-B-005-007).

Notes and references

1 C. L. Ventola, *Pharm. Ther.*, 2015, **40**, 277–283.
2 C. L. Ventola, *Pharm. Ther.*, 2015, **40**, 344–352.
3 M. Pasupuleti, A. Schmidtchen and M. Malmsten, *Crit. Rev. Biotechnol.*, 2012, **32**, 143–171.
4 S. Wang, P. A. Thacker, M. Watford and S. Qiao, *Curr. Protein Pept. Sci.*, 2015, **16**, 582–591.
5 L. Chopra, G. Singh, V. Choudhary and D. K. Sahoo, *Appl. Environ. Microbiol.*, 2014, **80**, 2981–2990.
6 M. N. Melo, R. Ferre and M. A. Castanho, *Nat. Rev. Microbiol.*, 2009, **7**, 245–250.
7 M. Pushpanathan, P. Gunasekaran and J. Rajendhran, *Int. J. Pept. Res. Therapeut.*, 2013, **2013**, 675391.
8 K. A. Brogden, *Nat. Rev. Microbiol.*, 2005, **3**, 238–250.
9 G. Wang, X. Li and Z. Wang, *Nucleic Acids Res.*, 2009, **37**, D933–D937.
10 G. Wang, X. Li and Z. Wang, *Nucleic Acids Res.*, 2016, **44**, D1087–D1093.
11 Z. Wang and G. Wang, *Nucleic Acids Res.*, 2004, **32**, D590–D592.
12 P. Staubitz, A. Peschel, W. F. Nieuwenhuizen, M. Otto, F. Gotz, G. Jung and R. W. Jack, *J. Pept. Sci.*, 2001, **7**, 552–564.
13 H. Jenssen, P. Hamill and R. E. Hancock, *Clin. Microbiol. Rev.*, 2006, **19**, 491–511.
14 A. A. Bahar and D. Ren, *Pharmaceuticals*, 2013, **6**, 1543–1575.
15 A. Tossi, L. Sandri and A. Giangaspero, *Biopolymers*, 2000, **55**, 4–30.
16 R. Ferre, M. N. Melo, A. D. Correia, L. Feliu, E. Bardaji, M. Planas and M. Castanho, *Biophys. J.*, 2009, **96**, 1815–1827.
17 H. G. Boman, *J. Intern. Med.*, 2003, **254**, 197–215.
18 R. E. Hancock, *Lancet Infect. Dis.*, 2001, **1**, 156–164.
19 M. R. Yeaman and N. Y. Yount, *Pharmacol. Rev.*, 2003, **55**, 27–55.
20 Y. Shai, *Biopolymers*, 2002, **66**, 236–248.
21 H. T. Chou, T. Y. Kuo, J. C. Chiang, M. J. Pei, W. T. Yang, H. C. Yu, S. B. Lin and W. J. Chen, *Int. J. Antimicrob. Agents*, 2008, **32**, 130–138.
22 B. J. Moncla, K. Pryke, L. C. Rohan and P. W. Graebing, *Adv. Biosci. Biotechnol.*, 2011, **2**, 404–408.
23 I. M. Torcato, Y. H. Huang, H. G. Franquelim, D. Gaspar, D. J. Craik, M. A. Castanho and S. Troeira Henriques, *Biochim. Biophys. Acta*, 2013, **1828**, 944–955.
24 M. L. Mangoni and Y. Shai, *Biochim. Biophys. Acta*, 2009, **1788**, 1610–1619.
25 M. L. Mangoni and Y. Shai, *Cell. Mol. Life Sci.*, 2011, **68**, 2267–2280.
26 I. Zelezetsky and A. Tossi, *Biochim. Biophys. Acta*, 2006, **1758**, 1436–1449.
27 E. Badosa, R. Ferre, M. Planas, L. Feliu, E. Besalu, J. Cabrefiga, E. Bardaji and E. Montesinos, *Peptides*, 2007, **28**, 2276–2285.
28 J. Turner, Y. Cho, N. N. Dinh, A. J. Waring and R. I. Lehrer, *Antimicrob. Agents Chemother.*, 1998, **42**, 2206–2214.
29 H. L. Chu, H. Y. Yu, B. S. Yip, Y. H. Chih, C. W. Liang, H. T. Cheng and J. W. Cheng, *Antimicrob. Agents Chemother.*, 2013, **57**, 4050–4052.
30 H. Mohanram and S. Bhattacharjya, *Biopolymers*, 2016, **106**, 345–356.
31 G. Laverty, S. P. Gorman and B. F. Gilmore, *Int. J. Mol. Sci.*, 2011, **12**, 6566–6596.
32 N. Y. Yount and M. R. Yeaman, *Annu. Rev. Pharmacol. Toxicol.*, 2012, **52**, 337–360.
33 S. Y. Wei, J. M. Wu, Y. Y. Kuo, H. L. Chen, B. S. Yip, S. R. Tzeng and J. W. Cheng, *J. Bacteriol.*, 2006, **188**, 328–334.
34 P. K. Lewis Kay and E. Tim Saarinen, *J. Am. Chem. Soc.*, 1992, **114**, 10663–10665.
35 F. Delaglio, S. Grzesiek, G. W. Vuister, G. Zhu, J. Pfeifer and A. Bax, *J. Biomol. NMR*, 1995, **6**, 277–293.
36 G. Wang, *Biochim. Biophys. Acta*, 2007, **1768**, 3271–3281.
37 G. Cornilescu, F. Delaglio and A. Bax, *J. Biomol. NMR*, 1999, **13**, 289–302.
38 A. T. Brunger, *Nat. Protoc.*, 2007, **2**, 2728–2733.
39 A. T. Brunger, P. D. Adams, G. M. Clore, W. L. DeLano, P. Gros, R. W. Grosse-Kunstleve, J. S. Jiang, J. Kuszewski, M. Nilges, N. S. Pannu, R. J. Read, L. M. Rice, T. Simonson and G. L. Warren, *Acta Crystallogr. Sect. D Biol. Crystallogr.*, 1998, **54**, 905–921.
40 R. A. Laskowski, J. A. Rullmannn, M. W. MacArthur, R. Kaptein and J. M. Thornton, *J. Biomol. NMR*, 1996, **8**, 477–486.
41 R. Koradi, M. Billeter and K. Wuthrich, *J. Mol. Graph.*, 1996, **14**(51–55), 29–32.
42 A. Bhunia, H. Mohanram and S. Bhattacharjya, *Biochim. Biophys. Acta*, 2012, **1818**, 1250–1260.
43 Y. J. Gordon, E. G. Romanowski and A. M. McDermott, *Curr. Eye Res.*, 2005, **30**, 505–515.
44 H. Kim, J. H. Jang, S. C. Kim and J. H. Cho, *J. Antimicrob. Chemother.*, 2014, **69**, 121–132.
45 F. D. Sonnichsen, J. E. Van Eyk, R. S. Hodges and B. D. Sykes, *Biochemistry*, 1992, **31**, 8790–8798.
46 A. P. Subasinghage, J. M. Conlon and C. M. Hewage, *Biochim. Biophys. Acta*, 2010, **1804**, 1020–1028.
47 I. Alana, J. P. Malthouse, F. P. O'Harte and C. M. Hewage, *Proteins*, 2007, **68**, 92–99.
48 E. Schrank, G. E. Wagner and K. Zangger, *Molecules*, 2013, **18**, 7407–7435.
49 J. Kyte and R. F. Doolittle, *J. Mol. Biol.*, 1982, **157**, 105–132.
50 E. F. Haney, H. N. Hunter, K. Matsuzaki and H. J. Vogel, *Biochim. Biophys. Acta*, 2009, **1788**, 1639–1655.
51 M. Lindberg and A. Graslund, *FEBS Lett.*, 2001, **497**, 39–44.
52 J. Lee and D. G. Lee, *J. Microbiol. Biotechnol.*, 2015, **25**, 759–764.

53 S. Bourbigot, E. Dodd, C. Horwood, N. Cumby, L. Fardy, W. H. Welch, Z. Ramjan, S. Sharma, A. J. Waring, M. R. Yeaman and V. Booth, *Biopolymers*, 2009, **91**, 1–13.
54 Z. Raja, S. Andre, C. Piesse, D. Sereno, P. Nicolas, T. Foulon, B. Oury and A. Ladram, *PLoS One*, 2013, **8**, e70782.
55 I. Y. Park, J. H. Cho, K. S. Kim, Y. B. Kim, M. S. Kim and S. C. Kim, *J. Biol. Chem.*, 2004, **279**, 13896–13901.
56 R. Saravanan, X. Li, K. Lim, H. Mohanram, L. Peng, B. Mishra, A. Basu, J. M. Lee, S. Bhattacharjya and S. S. Leong, *Biotechnol. Bioeng.*, 2014, **111**, 37–49.
57 K. Putsep, C. I. Branden, H. G. Boman and S. Normark, *Nature*, 1999, **398**, 671–672.
58 P. Bulet, R. Stocklin and L. Menin, *Immunol. Rev.*, 2004, **198**, 169–184.
59 A. Giangaspero, L. Sandri and A. Tossi, *Eur. J. Biochem.*, 2001, **268**, 5589–5600.
60 E. Barany-Wallje, A. Andersson, A. Graslund and L. Maler, *FEBS Lett.*, 2004, **567**, 265–269.
61 J. Jarvet, J. Zdunek, P. Damberg and A. Graslund, *Biochemistry*, 1997, **36**, 8153–8163.
62 M. Lindberg, H. Biverstahl, A. Graslund and L. Maler, *Eur. J. Biochem.*, 2003, **270**, 3055–3063.
63 A. P. Subasinghage, D. O'Flynn, J. M. Conlon and C. M. Hewage, *Biochim. Biophys. Acta*, 2011, **1808**, 1975–1984.
64 H. T. Chou, H. W. Wen, T. Y. Kuo, C. C. Lin and W. J. Chen, *Peptides*, 2010, **31**, 1811–1820.